



Original Paper

An adaptive finite-difference method for seismic traveltime modeling based on 3D eikonal equation



Bao-Ping Qiao ^{a, **}, Qing-Qing Li ^{b, *}, Wei-Guang He ^c, Dan Zhao ^a, Qu-Bo Wu ^a

^a CNNC Beijing Research Institute of Uranium Geology, Beijing 100029, China

^b National Key Laboratory of Deep Oil and Gas, China University of Petroleum (East China), Qingdao 266580, Shandong, China

^c SINOPEC Geophysical Research Institute, Nanjing, 211103, Jiangsu, China

ARTICLE INFO

Article history:

Received 15 November 2022

Received in revised form

24 June 2023

Accepted 14 September 2023

Available online 16 September 2023

Edited by Jie Hao and Meng-Jiao Zhou

Keywords:

3D eikonal equation

Accurate traveltimes

Global fast sweeping

3D inhomogeneous media

Adaptive finite-difference method

ABSTRACT

3D eikonal equation is a partial differential equation for the calculation of first-arrival traveltimes and has been widely applied in many scopes such as ray tracing, source localization, reflection migration, seismic monitoring and tomographic imaging. In recent years, many advanced methods have been developed to solve the 3D eikonal equation in heterogeneous media. However, there are still challenges for the stable and accurate calculation of first-arrival traveltimes in 3D strongly inhomogeneous media. In this paper, we propose an adaptive finite-difference (AFD) method to numerically solve the 3D eikonal equation. The novel method makes full use of the advantages of different local operators characterizing different seismic wave types to calculate factors and traveltimes, and then the most accurate factor and traveltime are adaptively selected for the convergent updating based on the Fermat principle. Combined with global fast sweeping describing seismic waves propagating along eight directions in 3D media, our novel method can achieve the robust calculation of first-arrival traveltimes with high precision at grid points either near source point or far away from source point even in a velocity model with large and sharp contrasts. Several numerical examples show the good performance of the AFD method, which will be beneficial to many scientific applications.

© 2023 The Authors. Publishing services by Elsevier B.V. on behalf of KeAi Communications Co. Ltd. This is an open access article under the CC BY license (<http://creativecommons.org/licenses/by/4.0/>).

1. Introduction

In local seismic exploration or global earthquake research, seismic first-arrival traveltimes are important for many applications such as seismic statics (Zhu et al., 2014), diving wave tomography (Meléndez et al., 2015; Feng et al., 2020; Yang et al., 2021), depth migration (Cheng et al., 2016), earthquake location (Li et al., 2018) and hydraulic fracturing induced seismicity monitoring (Tan et al., 2020). The eikonal equation, which is one part of the decompositions of seismic wave equation in high frequency, is the govern equation for the calculation of seismic first-arrival traveltimes (Engquist and Runborg, 2003). Because the eikonal equation is the static Hamilton-Jacobi equation with no analytical solution in general (Kao et al., 2005), many numerical methods such as ray tracing method (Červený and Hron, 1980), fast marching

level set method (Sethian, 1996), neural network method (Waheed et al., 2021) and finite-difference (FD) method (Vidale, 1988) have been developed to solve the eikonal equation for an accurate seismic first-arrival traveltimes in isotropic media with various velocity. For anisotropic (Alkhalifah, 1998, 2003; Stovas and Alkhalifah, 2012; Stovas, 2015; Berkar et al., 2022) and attenuate (Hao and Alkhalifah, 2017a, 2017b) media, accurate traveltimes can also be evaluated by solving the corresponding acoustic eikonal equations with developed numerical methods.

In the above numerical methods, FD method is a more efficient method and has been widely used for many scopes, such as transient electromagnetic modeling (Li and Huang, 2014), seismic wave simulation (Thorbecke and Draganov, 2011; Guo et al., 2022) and first-arrival traveltime calculation. Vidale first proposed FD method to rapidly solve the eikonal equation with 2D and 3D (Vidale, 1990) numerical models with slowly varying velocities, respectively. Although comparisons with ray tracing method showed that FD method can fulfill the calculation of first-arrival traveltimes with a higher precision, it still cannot guarantee the accurate solution of eikonal equation in a numerical model with strongly velocity contrasts due to the limitations of local operators. Based on FD

* Corresponding author.

** Corresponding author.

E-mail addresses: qiaobaoping@briug.cn (B.-P. Qiao), 20170069@upc.edu.cn (Q.-Q. Li).

operators, Zhao (2005) proposed fast sweeping (FS) method based on the Gauss-Seidel iterations to solve the eikonal equation. FS method is simple to implement for a monotonous and stable solution of first-arrival traveltimes due to the Godunov-type numerical flux. Because local operators based on 2 point local operator only consider the propagation of plane waves, FS method with first-order accuracy is suitable for the grid points far away from source point (Lu and Zhang, 2022) and induces great errors near source point due to source singularity. To avoid the singularity of source point, Fomel et al. (2009) used multiplicative factor decomposition (MFD) method to solve the eikonal equation in a 2D numerical model and significantly improved the calculation accuracy of first-arrival traveltimes at the grid points near source point due to the accurate characterization of spherical wave fronts. Combined with the advantages of factored eikonal equation, Noble et al. (2014) proposed a 3D hybrid FD method with a window surrounding source point to solve the eikonal equation. The hybrid FD method by using spherical wave operators inside the window and plane wave operators outside the window can fulfill an accurate calculation of seismic traveltimes in heterogeneous slowness model. However, the artificial selection of different local operators cannot choose the most accurate operators to characterize different wave types propagating along different directions for each grid point. To solve the above problem, Qiao et al. (2021) proposed an adaptive finite-difference (AFD) method to automatically select the most accurate 2D local operators and fulfill the efficient and robust calculation of first-arrival traveltimes in 2D media with extremely complex velocity parameters. Because seismic waves actually propagate along 3D directions in realistic physical world, the 2D eikonal equation cannot characterize all the possible seismic wave types propagating in a 3D model and thus reduces the accuracy of first-arrival traveltimes simulated by 2D AFD method.

Based on the above analysis, this paper extends the AFD method for 2D complex media to a more general AFD schemes for the 3D eikonal equation. Combined with the Fermat principle and global fast sweeping schemes, the novel method makes an adaptive choice of different 3D local operators characterizing different seismic wave propagations to calculate a more accurate and robust first-arrival traveltimes in strongly heterogeneous media, which will be beneficial to seismic monitoring, tomographic imaging and earthquake location. The rest of paper is organized as follows. First, we introduce the candidate 3D local operators representing different seismic wave propagations for the 3D eikonal equation. Second, the AFD method is presented to accurately calculate 3D first-arrival traveltimes. Thirdly, three numerical examples are solved to show the stable and robust performance of the novel method. Lastly, we present the discussion and conclusions.

2. Local operators

The analytical eikonal equation is a non-linear partial differential equation generally expressed as

$$\begin{cases} |\nabla T(X)| = S(X), X \in \Omega, \\ T(X) = 0, X \in \partial\Omega, \end{cases} \quad (1)$$

where $\Omega \subset R^n$ represent an n dimensional domain, X is the space variable, $S(X)$ is the slowness model (the inverse of velocity model), $T(X)$ is the first-arrival traveltimes, ∇ is the Hamilton operator.

For 3D numerical simulation, we first discretize the 3D slowness model in the Cartesian coordinates with a grid interval of d_x , d_y and d_z along x , y and z direction, respectively. The discretized slowness model consists of $N_x \times N_y \times N_z$ grid points in total. After the above numerical discretization, Fig. 1 shows that first-arrival traveltimes are located at the vertices of grid cells and a constant slowness

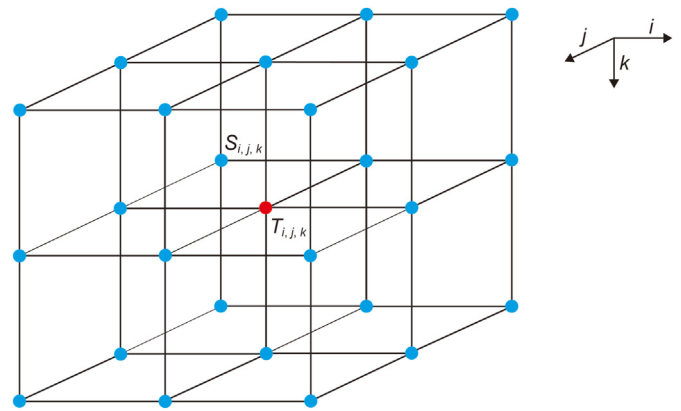


Fig. 1. 3D diagram shows the traveltime distributions at different grid points and slowness distributions in different grid cells. Red dot represents the traveltime $T_{i,j,k}$ to be solved and blue dots represent the traveltimes used for the solution of traveltime indicated by red dot. Symbol $S_{i,j,k}$ indicates the constant slowness in grid cell.

value is assigned for each grid cell. In this paper, the novel method uses five different local operators to calculate the above discretized first-arrival traveltimes. For simplicity, only the grid cell with constant slowness $S_{i,j,k}$ shown in Fig. 1 is used for the derivations of local operators to characterize different seismic waves propagating along different directions for the solution of first-arrival traveltimes. The local operators for the other seven grid cells shown in Fig. 1 also are simply derived with the similar steps to characterize different seismic waves propagating along the other seven directions.

2.1. Plane wave 8 point operator

Vidale (1990) showed that 8 point operator is more accurate than other operators for the modeling of seismic traveltimes generated by seismic transmitted plane waves. As shown in Fig. 2, we use eight grid points for the grid cell filled with a constant slowness $S_{i,j,k}$ to simulate the traveltime $T_{i,j,k}$ located at grid point (x_i, y_j, z_k) . Then, the three partial derivatives along 3D spatial

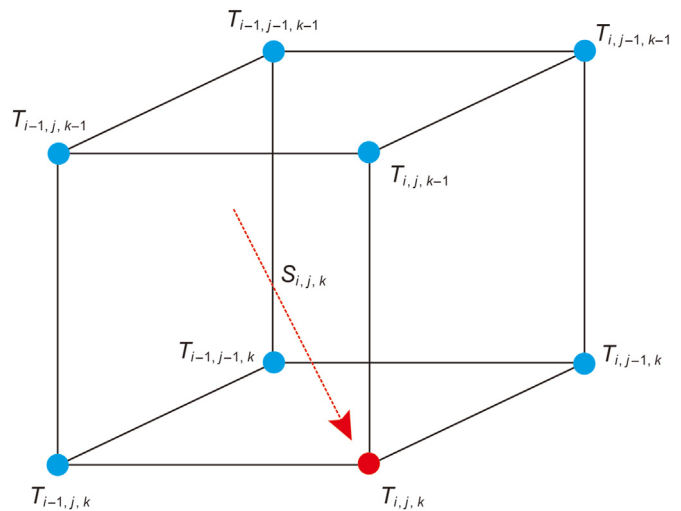


Fig. 2. 3D diagram of plane wave 8 point operator. Symbols with capital letter T represent traveltime distributions at different grid points and symbol with capital letter S indicates slowness distribution in grid cell. Red dotted arrow indicates plane seismic waves propagating in grid cell. The traveltime indicated by red dot is simulated by using the traveltimes indicated by blue dots.

directions in Eq. (1) are evaluated by the following FD formulas:

$$\frac{\partial T}{\partial x} = \frac{T_{i,j,k} - T_{px}}{4d_x}, \quad (2)$$

$$\frac{\partial T}{\partial y} = \frac{T_{i,j,k} - T_{py}}{4d_y}, \quad (3)$$

$$\frac{\partial T}{\partial z} = \frac{T_{i,j,k} - T_{pz}}{4d_z}, \quad (4)$$

where the intermediate variables T_{px} , T_{py} and T_{pz} are defined as:

$$T_{px} = T_{i-1,j,k} - T_{i,j,k} + T_{i-1,j-1,k} - T_{i,j,k-1} + T_{i-1,j,k-1} - T_{i,j-1,k-1} + T_{i-1,j-1,k-1}, \quad (5)$$

$$T_{py} = T_{i,j-1,k} - T_{i,j,k} + T_{i-1,j-1,k} - T_{i,j,k-1} + T_{i,j-1,k-1} - T_{i-1,j,k-1} + T_{i-1,j-1,k-1}, \quad (6)$$

$$T_{pz} = T_{i,j,k-1} - T_{i,j,k} + T_{i-1,j,k-1} - T_{i,j-1,k} + T_{i,j-1,k-1} - T_{i-1,j-1,k} + T_{i-1,j-1,k-1}. \quad (7)$$

Then, Eq. (1) can be discretized as:

$$\left(\frac{T_{i,j,k} - T_{px}}{4d_x}\right)^2 + \left(\frac{T_{i,j,k} - T_{py}}{4d_y}\right)^2 + \left(\frac{T_{i,j,k} - T_{pz}}{4d_z}\right)^2 = S_{i,j,k}^2. \quad (8)$$

The above equation is an quadratic equation with one unknown variable $T_{i,j,k}$ and gives the following solution,

$$T_{i,j,k} = \frac{-b \pm \sqrt{b^2 - 4ac}}{2a}, \quad (9)$$

$$a = \frac{1}{16} \left(\frac{1}{d_x^2} + \frac{1}{d_y^2} + \frac{1}{d_z^2} \right), \quad (10)$$

$$b = -\frac{1}{8} \left(\frac{T_{px}}{d_x^2} + \frac{T_{py}}{d_y^2} + \frac{T_{pz}}{d_z^2} \right), \quad (11)$$

$$c = \frac{1}{16} \left(\frac{T_{px}^2}{d_x^2} + \frac{T_{py}^2}{d_y^2} + \frac{T_{pz}^2}{d_z^2} \right) - S_{i,j,k}^2. \quad (12)$$

Because the solutions for Eq. (8) need to satisfy the illumination condition (Podvin and Lecomte, 1991), the discriminant under the square root is a positive number, which gives,

$$b^2 - 4ac \geq 0. \quad (13)$$

Meanwhile, only the larger root in Eq. (9) is chosen for the solution of traveltime due to the causality condition (Fomel et al., 2009). From the above analysis, we can calculate the first-arrival traveltime $T_{i,j,k}$ from transmitted plane wave propagating along the direction indicated by red dotted arrow with the other seven neighboring grid points as shown in Fig. 2. However, the plane wave 8 point operator can only be used to accurately calculate the traveltimes generating from plane wave fronts transmitting in grid cell.

2.2. Plane wave 4 point operator

Besides the plane waves transmitting in grid cell, there are still plane waves propagating along the three faces as the red dotted arrows shown in Fig. 3. The plane wave 4 point operator can be used to accurately simulate the first-arrival traveltime $T_{i,j,k}$ generating from plane waves propagating parallel with the three faces. For simplicity, we use the bottom face $z = k$ to calculate the plane wave 4 point operator. Then, the two partial derivatives with respect to x and y directions in Eq. (1) are numerically evaluated as

$$\frac{\partial T}{\partial x} = \frac{T_{i,j,k} - T_{px}}{2d_x}, \quad (14)$$

$$\frac{\partial T}{\partial y} = \frac{T_{i,j,k} - T_{py}}{2d_y}, \quad (15)$$

where the intermediate variables T_{px} and T_{py} are defined as:

$$T_{px} = T_{i-1,j,k} - T_{i,j-1,k} + T_{i-1,j-1,k}, \quad (16)$$

$$T_{py} = T_{i,j-1,k} - T_{i-1,j,k} + T_{i-1,j-1,k}. \quad (17)$$

Then, Eq. (1) can be discretized as:

$$\left(\frac{T_{i,j,k} - T_{px}}{2d_x}\right)^2 + \left(\frac{T_{i,j,k} - T_{py}}{2d_y}\right)^2 = S_m^2, \quad (18)$$

$$S_m = \min(S_{i,j,k}, S_{i,j,k+1}), \quad (19)$$

where min function represents evaluating the minimum one from different values. The above equation is also an quadratic equation for variable $T_{i,j,k}$ and gives the following solution,

$$T_{i,j,k} = \frac{-b \pm \sqrt{b^2 - 4ac}}{2a}, \quad (20)$$

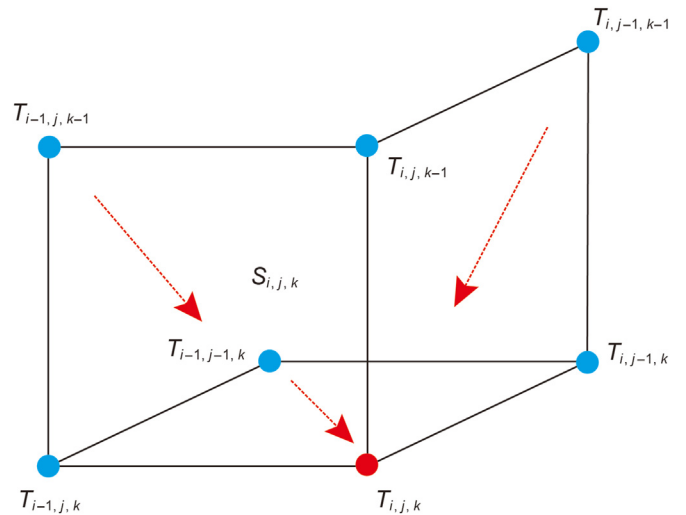


Fig. 3. 3D diagram of plan and spherical wave 4 point operators. Symbols with capital letter T represent traveltime distributions at different grid points and symbol with capital letter S indicates slowness distribution in grid cell. Red dotted arrows indicate plane or spherical seismic waves propagating parallel with grid faces. The traveltime indicated by red dot is simulated by using the traveltimes indicated by blue dots.

$$a = \frac{1}{4} \left(\frac{1}{d_x^2} + \frac{1}{d_y^2} \right), \quad (21)$$

$$b = -\frac{1}{2} \left(\frac{T_{px}}{d_x^2} + \frac{T_{py}}{d_y^2} \right), \quad (22)$$

$$c = \frac{1}{4} \left(\frac{T_{px}^2}{d_x^2} + \frac{T_{py}^2}{d_y^2} \right) - S_m^2. \quad (23)$$

The illumination condition (Podvin and Lecomte, 1991) also results in a positive number of the discriminant under the square root in Eq. (20) and the causality condition (Fomel et al., 2009) only choose the larger root in Eq. (20) for the solution of traveltime generated by the plane wave propagating parallel with the bottom face. The traveltimes generated by the plane waves propagating along the other two faces also can be simply derived with the similar steps. Then, the minimum traveltime is selected from traveltimes calculated from the three faces as the solution of traveltime for the grid point $T_{i,j,k}$ as the red dot shown in Fig. 3, which indicates that the plane wave 4 point operator can only be used to accurately calculate the traveltimes generating from plane waves parallel with the three faces surrounding the grid point to be solved.

2.3. Spherical wave 2 point operator

Because the above two plane wave operators cannot handle the singularity of source point, plane wave operators will calculate the first-arrival traveltimes generated from spherical waves with low precision, which induce that traveltime error increases as the distance between calculated grid point and source point decreases. To reduce the big errors induced by source singularity, Fomel et al. (2009) used multiplicative factor decomposition to represent traveltimes and slowness model as,

$$\begin{cases} T(X) = T_0(X)\tau(X), \\ S(X) = S_0(X)\alpha(X), \end{cases} \quad (24)$$

where $\tau(X)$ and $\alpha(X)$ represent the multiplicative factors of traveltimes and slowness, respectively. $T_0(X)$ and $S_0(X)$ also satisfy the eikonal equation as,

$$\begin{cases} |\nabla T_0(X)| = S_0(X), X \in \Omega, \\ T_0(X) = 0, X \in \partial\Omega. \end{cases} \quad (25)$$

For a constant gradient or constant slowness model $S_0(X)$, an analytical solution for $T_0(X)$ will be simply evaluated from Eq. (25). Then, combined with Eq. (24), Eq. (1) is transformed into an equation about the factor $\tau(X)$ as follows,

$$T_0^2 |\nabla \tau|^2 + 2T_0 \tau \nabla T_0 \cdot \nabla \tau + (\tau^2 - \alpha^2) S_0^2 = 0, X \in \Omega, \quad (26)$$

with the boundary conditions:

$$\tau(X) = \begin{cases} T(X)/T_0(X), T_0(X) \neq 0 \\ \alpha(X)T_0(X) = 0 \end{cases}, \quad (27)$$

$X \in \partial\Omega$.

For stability and convergence (Fomel et al., 2009), a two point FD operator is used to calculate the traveltimes from transmitted spherical waves as the red dotted arrow shown in Fig. 4. Then,

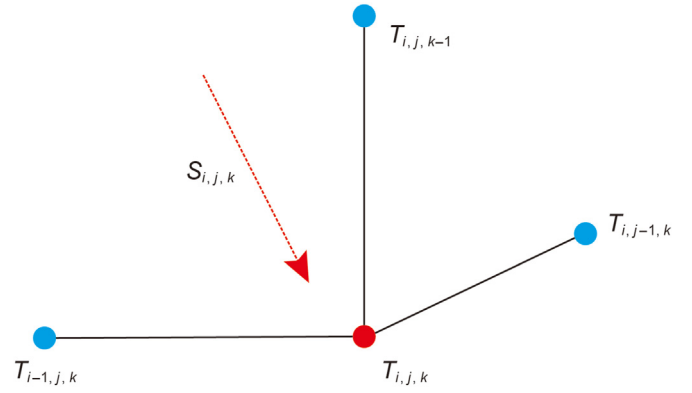


Fig. 4. 3D diagram of spherical wave 2 point operator. Symbols with capital letter T represent traveltime distributions at different grid points and symbol with capital letter S indicates slowness distribution in grid cell. Red dotted arrow indicates spherical seismic waves propagating in grid cell. The traveltime indicated by red dot is simulated by using the traveltimes indicated by blue dots.

based on spherical wave 2 point operator, the three partial derivatives of $\tau(X)$ with respect to x, y and z directions in Eq. (26) are evaluated by the following FD formulas:

$$\frac{\partial \tau}{\partial x} = \frac{\tau_{i,j,k} - \tau_{sx}}{d_x}, \quad (28)$$

$$\frac{\partial \tau}{\partial y} = \frac{\tau_{i,j,k} - \tau_{sy}}{d_y}, \quad (29)$$

$$\frac{\partial \tau}{\partial z} = \frac{\tau_{i,j,k} - \tau_{sz}}{d_z}, \quad (30)$$

where the intermediate variables τ_{sx} , τ_{sy} and τ_{sz} are derived by replacing variable T with τ in Fig. 4,

$$\tau_{sx} = \tau_{i-1,j,k}, \quad (31)$$

$$\tau_{sy} = \tau_{i,j-1,k}, \quad (32)$$

$$\tau_{sz} = \tau_{i,j,k-1}. \quad (33)$$

Then, Eq. (26) becomes a quadratic equation for the one unknown variable $\tau_{i,j,k}$ and gives the following solution,

$$\tau_{i,j,k} = \frac{-b \pm \sqrt{b^2 - 4ac}}{2a}, \quad (34)$$

$$a = T_0^2 \left(\frac{1}{d_x^2} + \frac{1}{d_y^2} + \frac{1}{d_z^2} \right) + 2T_0 \left(\frac{T_{0,x}}{d_x} + \frac{T_{0,y}}{d_y} + \frac{T_{0,z}}{d_z} \right) + S_0^2, \quad (35)$$

$$b = -2T_0^2 \left(\frac{\tau_{sx}}{d_x^2} + \frac{\tau_{sy}}{d_y^2} + \frac{\tau_{sz}}{d_z^2} \right) - 2T_0 \left(\frac{\tau_{sx}T_{0,x}}{d_x} + \frac{\tau_{sy}T_{0,y}}{d_y} + \frac{\tau_{sz}T_{0,z}}{d_z} \right), \quad (36)$$

$$c = T_0^2 \left(\frac{\tau_{sx}^2}{d_x^2} + \frac{\tau_{sy}^2}{d_y^2} + \frac{\tau_{sz}^2}{d_z^2} \right) - S_{i,j,k}^2, \quad (37)$$

with the illumination condition,

$$b^2 - 4ac \geq 0. \quad (38)$$

where $T_{0,x}$, $T_{0,y}$ and $T_{0,z}$ represent the derivatives of T_0 along x , y and z directions, respectively. To solve source singularity, $S_0(X)$ is set to be a slowness model with homogeneous parameter, which is equal to the slowness value at source point. Then, $T_0(X)$ is analytically solved for the entire constant slowness model. With the solutions of $S_0(X)$ and $T_0(X)$, Eqs. (34) and (24) can be used to numerically simulate the factor $\tau_{i,j,k}$ and traveltime $T_{i,j,k}$ for each grid point in sequence. Due to the causality condition (Fomel et al., 2009), only the calculated traveltime $T_{i,j,k}$ larger than the neighboring three traveltimes as the blue dots shown in Fig. 4 is selected for traveltime and factor updating.

From above analysis, we conclude that the first-arrival traveltimes generated by transmitted spherical waves propagating along the direction indicated by red dotted arrow in grid cell as shown in Fig. 4 can be calculated from the three neighboring grid points. Because source singularity is captured by using easily computed multiplicative factors, the spherical wave 2 point operator can more accurately calculate the first-arrival traveltime from transmitted spherical waves near source point.

2.4. Spherical wave 4 point operator

Besides the spherical waves transmitting in grid cell, there are still spherical waves propagating parallel with the three faces as the red dotted arrows shown in Fig. 3. Spherical wave 4 point operator can be used to accurately calculate the first-arrival traveltime $T_{i,j,k}$ from spherical waves propagating parallel with the three faces. We also use the bottom face $z = k$ as shown in Fig. 3 to derive spherical wave 4 point operator. For FD scheme, the two numerical partial derivatives of $\tau(X)$ with respect to x and y directions and two intermediate variables τ_x and τ_y are easily evaluated just by replacing variable T with τ from Eqs. (14)–(17). Then, Eqs. (26) and (27) are discretized and give the following solution,

$$\tau_{i,j,k} = \frac{-b \pm \sqrt{b^2 - 4ac}}{2a}, \quad (39)$$

$$a = \frac{T_0^2}{4} \left(\frac{1}{d_x^2} + \frac{1}{d_y^2} \right) + T_0 \left(\frac{T_{0,x}}{d_x} + \frac{T_{0,y}}{d_y} \right) + S_0^2, \quad (40)$$

$$b = -\frac{T_0^2}{2} \left(\frac{\tau_{sx}}{d_x^2} + \frac{\tau_{sy}}{d_y^2} \right) - T_0 \left(\frac{\tau_{sx} T_{0,x}}{d_x} + \frac{\tau_{sy} T_{0,y}}{d_y} \right), \quad (41)$$

$$c = \frac{T_0^2}{4} \left(\frac{\tau_{sx}^2}{d_x^2} + \frac{\tau_{sy}^2}{d_y^2} \right) - S_m^2. \quad (42)$$

$$S_m = \min(S_{i,j,k}, S_{i,j,k+1}), \quad (43)$$

where $T_{0,x}$ and $T_{0,y}$ represent the derivatives of T_0 with respect to x

and y directions, respectively. $T_0(X)$ also has an analytical solution for a model $S_0(X)$ with constant slowness value at source point. As introduced in section 2.3, only the larger calculated traveltime $T_{i,j,k}$ is selected for the solution of traveltime generated by the spherical wave propagating parallel with the bottom face. The spherical wave 4 point operator used for the other two faces also can be simply derived with the similar steps. Then, the minimum traveltime is selected from traveltimes evaluated from the three faces as the solution of traveltime for the grid point as the red dot shown in Fig. 3, which indicates that spherical wave 4 point operator can be used to accurately calculate the traveltimes generating from spherical waves propagating parallel with faces for the grid points near source point.

2.5. Refracted wave 2 point operator

Besides plane waves and spherical waves, there are still refracted waves or direct waves propagating along the edges as the red dotted arrows shown in Fig. 5 for each grid cell. To accurately simulate the first-arrival traveltimes generating from refracted waves or directed waves, we use refracted wave 2 point operator based on the grid cell shown in Fig. 5:

$$T_{i,j,k} = \min(T_{rx}, T_{ry}, T_{rz}), \quad (44)$$

$$T_{rx} = T_{i-1,j,k} + d_x \min(S_{i,j,k}, S_{i,j+1,k}, S_{i,j,k+1}, S_{i,j+1,k+1}), \quad (45)$$

$$T_{ry} = T_{i,j-1,k} + d_y \min(S_{i,j,k}, S_{i+1,j,k}, S_{i,j,k+1}, S_{i+1,j,k+1}), \quad (46)$$

$$T_{rz} = T_{i,j,k-1} + d_z \min(S_{i,j,k}, S_{i+1,j,k}, S_{i,j+1,k}, S_{i+1,j+1,k}). \quad (47)$$

Then, the first-arrival traveltime $T_{i,j,k}$ can be simulated with the three neighboring traveltimes $T_{i-1,j,k}$, $T_{i,j-1,k}$ and $T_{i,j,k-1}$. Therefore, the local refracted wave 2 point operator is able to accurately simulate the first-arrival traveltimes generated by refracted waves or direct waves propagating along grid edges.

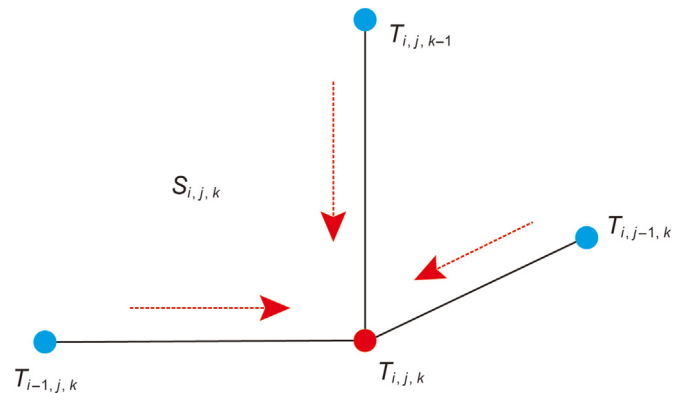


Fig. 5. 3D diagram of refracted wave 2 point operator. Symbols with capital letter T represent traveltime distributions at different grid points and symbol with capital letter S indicates slowness distribution in grid cell. Red dotted arrows indicate refracted or direct waves propagating along grid edges. The traveltime indicated by red dot is simulated by using the traveltimes indicated by blue dots.

3. AFD schemes

Based on the local operators introduced in section 2, we can calculate the first-arrival traveltimes $T_{i,j,k}$ generated from different seismic waves propagating in the grid cell with constant slowness $S_{i,j,k}$ shown in Fig. 1. There also are the other seven grid cells to calculate seismic traveltimes $T_{i,j,k}$ generated from seismic waves propagating from the other seven directions. To take into account all the possible propagation directions of different seismic waves, AFD method is proposed to calculate the most accurate first-arrival traveltimes in strongly contrasted slowness parameters with unconditional convergence based on the Fermat principle. The novel method in detail is as follows.

1. Initialization: for source point locating at grid vertex, traveltimes T and factor τ for the grid vertex assigned to source point are set to be 0 and 1, respectively. For source point not locating at grid vertex, exact traveltimes and factors for the grid vertices just surrounding source point are analytically extrapolated by using constant slowness parameters. The above exact initialized values are not updated in next steps. For all the other grid vertices, traveltimes and factors are set to be a big positive number V_{\max} , which will be updated in the following iteration.
2. Globally fast sweep the entire domain ($N_x \times N_y \times N_z$ grid points) along eight alternating directions repeatedly with Gauss-Seidel iterations.
 - (1) $i = 2: N_x; j = 2: N_y; k = 2: N_z$,
 - (2) $i = 2: N_x; j = 2: N_y; k = N_z - 1: 1$,
 - (3) $i = N_x - 1: 1; j = 2: N_y; k = 2: N_z$,
 - (4) $i = N_x - 1: 1; j = 2: N_y; k = N_z - 1: 1$,
 - (5) $i = 2: N_x; j = N_y - 1: 1; k = 2: N_z$,
 - (6) $i = 2: N_x; j = N_y - 1: 1; k = N_z - 1: 1$,
 - (7) $i = N_x - 1: 1; j = N_y - 1: 1; k = 2: N_z$,
 - (8) $i = N_x - 1: 1; j = N_y - 1: 1; k = N_z - 1: 1$.
3. During each sweeping direction, different local operators corresponding to the specified sweeping direction are used for the modeling of first-arrival traveltimes T and factor τ at each grid point based on the adaptive updating schemes as follows:
 - (1) Calculate traveltimes T_{p8} by plane wave 8 point operator. If real root exists, T_{p8} is identical to the real root; otherwise, $T_{p8} = V_{\max}$.
 - (2) Calculate traveltimes T_{p4} by plane wave 4 point operator. If real root exists, T_{p4} is identical to the real root; otherwise, $T_{p4} = V_{\max}$.
 - (3) Calculate traveltimes T_{s2} by spherical wave 2 point operator. If real root exists, T_{s2} is identical to the real root; otherwise, $T_{s2} = V_{\max}$.
 - (4) Calculate traveltimes T_{s4} by spherical wave 4 point operator. If real root exists, T_{s4} is identical to the real root; otherwise, $T_{s4} = V_{\max}$.
 - (5) Calculate traveltimes T_{r2} by refracted wave 2 point operator.
 - (6) Select the minimum value from the above five calculate traveltimes for candidate traveltimes $T_{\text{can}} = \min(T_{p8}, T_{p4}, T_{s2}, T_{s4}, T_{r2})$.
 - (7) Based on the Fermat principle, only when the candidate traveltimes T_{can} is smaller than the old traveltimes T_{old} , the candidate traveltimes is selected for the updated traveltimes T_{upd} and updating of factor.
4. Repeat steps 2 and 3 for each iteration until first-arrival traveltimes convergent to stable solutions, the convergence criterion for each iteration is as,

$$\|T_{\text{upd}} - T_{\text{old}}\|_{\infty} < \delta, \quad (48)$$

where $\|\cdot\|_{\infty}$ is an infinite norm operator, δ is a very small positive number which is assigned to be $1\text{E}-6$ in the following numerical examples.

From the above algorithm flow, we know that AFD method simultaneously uses different local operators to calculate traveltimes from different seismic wave types and global fast sweepings cover all the possible propagating directions of seismic waves in a 3D inhomogeneous media. Then, the minimum traveltimes are adaptively selected as the most accurate solution of the 3D eikonal equation based on the Fermat principle. The causality condition and Gauss-Seidel iteration guarantee the iterative solution converges to the stable solution of discretized 3D eikonal equation. Thus, AFD method can fulfill the accurate and robust calculation of first-arrival traveltimes for any strongly heterogeneous media.

4. Numerical examples

In this section, three numerical results are illustrated to show the good performance of our AFD method. T_0 is set to be a distance function for local spherical wave operators in the following numerical examples.

4.1. Example 1

We use a 3D homogeneous slowness model with a constant velocity of 2000 m/s to calculate the seismic first-arrival traveltimes with the 3D eikonal equation. There are 100 grid cells with a grid spacing of 10 m for each direction, which generate a 3D cubic of 1000 m \times 1000 m \times 1000 m. Source point is deployed at the grid point (500 m, 500 m, 500 m). Based on boundary condition, we can simply evaluate the analytical first-arrival traveltimes and further calculate absolute traveltimes errors by using different numerical methods. Eq. (49) is used for the absolute traveltimes error calculation in the following examples.

$$\Delta T = |T_a - T_n|, \quad (49)$$

where ΔT represents the absolute errors, T_a and T_n represent the analytical and numerical solutions, respectively.

Firstly, the first-arrival traveltimes calculated by FS method are used to generate the absolute traveltimes errors with Eq. (49). As the blue areas shown in Fig. 6a and 6b, FS method generates relatively small traveltimes errors only near the three axes passing through source point due to the only using of plane wave 2 point operator (Zhao, 2005). Because plane wave operator cannot accurately handle the problems induced by source singularity, the absolute traveltimes error not along axes rapidly increases as the distance between source point and grid point increases, which induces a maximum traveltimes error of $1.14\text{E}-2$ s shown in Table 1. After the capture of source singularity by using spherical wave 2 point operator (Fomel et al., 2009), MFD method is adopted to handle the spherical wave propagation and generate the absolute traveltimes errors shown in Fig. 6c and 6d. Compared with Fig. 6a and 6b, it is clearly observed that the traveltimes errors have been significantly reduced to a quantity of 10^{-4} s. The blue lines in Fig. 6c and three blue faces in Fig. 6d prove that the traveltimes located on the three faces passing through source point are almost identical to the analytical solutions due to the using of spherical wave operators. Meanwhile, the traveltimes error also gradually increases as the

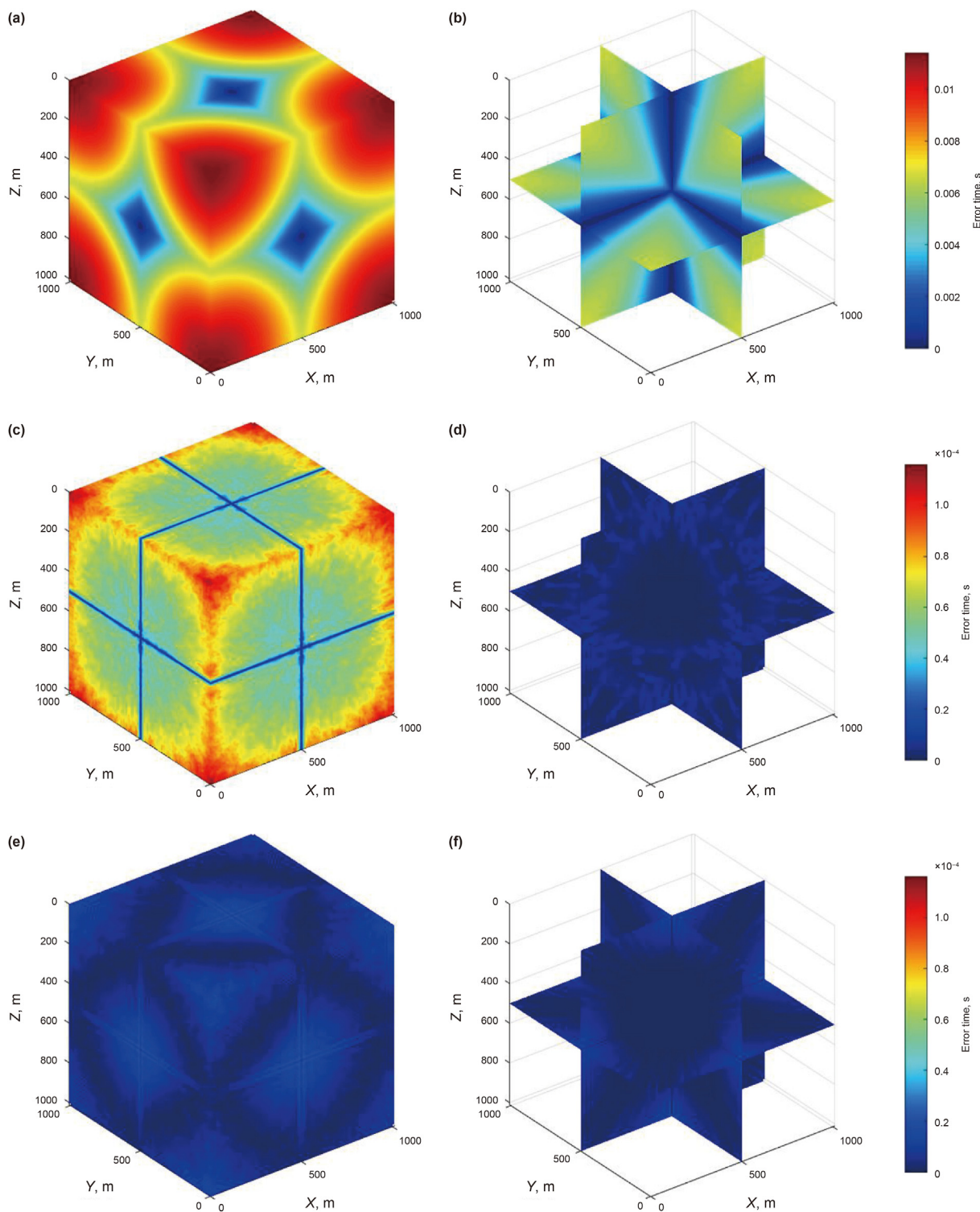


Fig. 6. Absolute traveltime errors in 3D homogeneous media by FS method on faces passing through the grid points (0 m, 0 m, 0 m) (a) and (500 m, 500 m, 500 m) (b), MFD method on faces passing through the grid points (0 m, 0 m, 0 m) (c) and (500 m, 500 m, 500 m) (d), and AFD method on faces passing through the grid points (0 m, 0 m, 0 m) (e) and (500 m, 500 m, 500 m) (f).

Table 1
The maximum absolute traveltime errors and computational costs in **example 1**.

Methods	FS	MFD	AFD
Maximum errors, s	1.140E-2	1.160E-4	2.235E-5
CPU time, s	0.618	36.284	2.390

distance between calculated grid point and source point increases, which induces relatively big traveltime errors with a maximum value of $1.16E-4$ s shown in **Table 1**. Finally, **Fig. 6e** and **6f** indicates that AFD method further reduces traveltime errors with a maximum value of $2.235E-5$ s shown in **Table 1**, because the adaptively updating schemes automatically select the most

accurate local operators for different seismic wave types. Table 1 also shows that FS method with the lowest accuracy of traveltime only takes the least computational cost for the numerical solution due to the only using of plane wave operator. Although the number of local operators in MFD method is less than the number of local operators in AFD method, MFD still takes the most computational cost of 36.284 s. The reason is that AFD method uses five different operators to adaptively select the most accurate one in one iteration, the number of iterations for AFD method is significantly fewer than the number of iterations for MFD method, which results in that AFD method converges to the stable solution much faster than MFD method. Thus, the above results show that our novel method can rapidly calculate the most accurate and stable first-arrival traveltimes in 3D homogeneous media.

4.2. Example 2

For most media below the Earth surface, slowness decreases as the depth below the Earth surface increases. Therefore, this example builds a more realistic 3D slowness model with a constant slowness distribution of 2 s/km at the surface $z = 0$ and a constant gradient of slowness squared by a gradient of -2.9 s/km along the depth $z > 0$. There are 100 grid cells with a grid spacing of 5 m for each direction, which generate a 3D cubic of $500\text{ m} \times 500\text{ m} \times 500\text{ m}$. Source point is deployed at the origin coordinate (0 m, 0 m, 0 m). Based on boundary condition and the generated slowness model, the analytical first-arrival traveltimes are simply evaluated as shown in Fig. 7. We clearly observe that analytical traveltimes are symmetrically distributed along both sides of z axis, and the traveltimes along z direction is smaller than the traveltimes along x and y directions for grid points at the identical distances away from source point due to the decrease of slowness along z direction.

We use FS method to calculate first-arrival traveltimes and absolute traveltime errors based on Eq. (49). Like the analytical solutions, Fig. 8a and 8b shows that the traveltime errors also are symmetrically distributed along both sides of z axis. Because plane wave operator only accurately characterizes the propagations of plane wave fronts, the relatively small traveltime errors are only distributed near the three axes passing through source point as the blue area showing in Fig. 8a and traveltime error also gradually

increases as the distance from source increases. Table 2 shows that although the maximum traveltime error generated by FS method is only $2.26\text{E}-2$ s, the number of traveltime errors greater than 0.01 s is up to 85.4%, which induce the wide warm area shown in Fig. 8a and 8b. After the solution of source singularity by MFD method, the warm area in Fig. 8c are reduced due to the accurately characterized spherical wave front. Compared with Fig. 8b and d also shows wide warm area with a bigger maximum traveltime error of $2.483\text{E}-1$ s at the farthest grid point (500 m, 500 m, 500 m), which are induced by the only using of spherical wave 2 point operator at far offset (Fomel et al., 2009). As shown in Table 2, the number of traveltime errors greater than 0.01 s is almost the same as the result simulated by FS method and the computational cost of MFD method is only slightly greater than the computational cost of FS method. From the above results, we conclude that MFD method is a more accurate method than FS method for grid points near source point by using spherical wave operators. However, because seismic spherical waves at near offset gradually convert to plane waves at far offset, the accuracy of MFD method decreases faster than FS method as the distance from source increases. The above problems are solved very well by AFD method due to the adaptive selection of different local operators for different wave types. Fig. 8e shows that traveltime errors on the three faces passing through source point are relatively smaller than the results shown in Fig. 8c and 8f also shows a much colder area with a maximum traveltime error almost identical to the maximum value shown in Fig. 8b. Meanwhile, Table 2 shows that the number of traveltime errors greater than 0.01 s has been significantly reduced to 46.6% with a time consumption of only 16.8 s, which is the least computational cost than the other two methods. Therefore, AFD method can accurately and fast calculate seismic first-arrival traveltimes simultaneously at near and far wavefields for a realistic 3D inhomogeneous model.

For seismic wave propagating in arbitrarily heterogeneous 3D media, we know that seismic wave types will gradually are converted from spherical waves at near source point to plane waves far away from source point. Because seismic spherical waves, plane waves and refracted waves propagating along different 3D directions all exist at near source point, our AFD method can adaptively select appropriate local operators to calculate the most accurate first-arrival traveltimes than FS and MFD method near source point. As distance from source point increases, plane waves

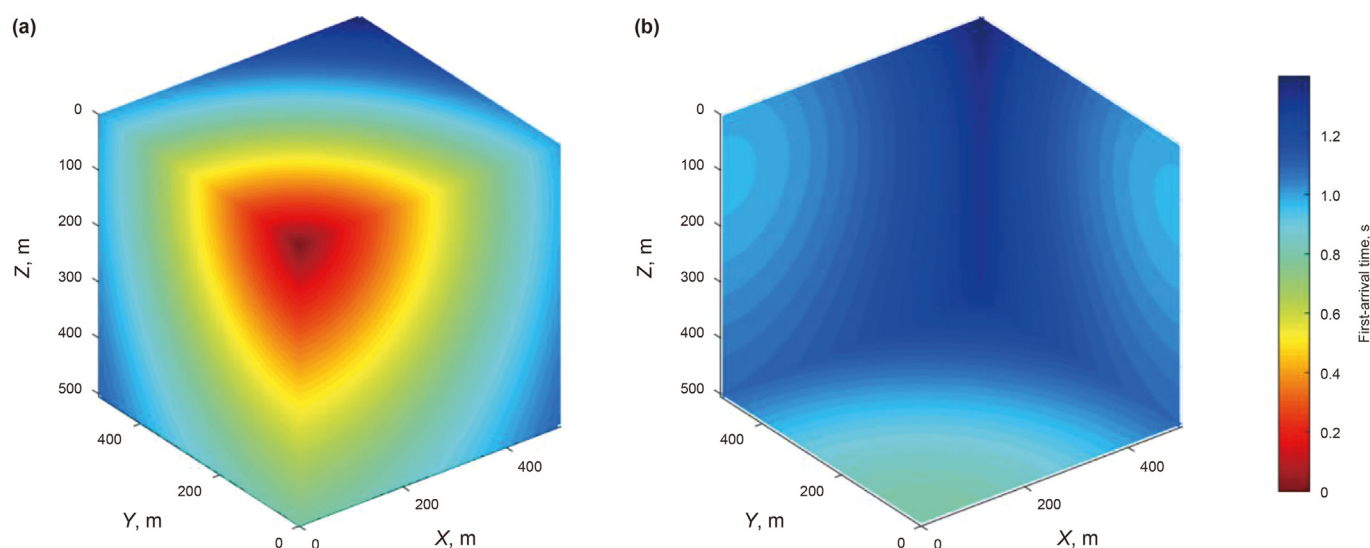


Fig. 7. Analytical traveltimes simulated from a 3D model with constant gradient of slowness squared on faces passing through the grid points (0 m, 0 m, 0 m) (a) and (500 m, 500 m) (b), respectively.

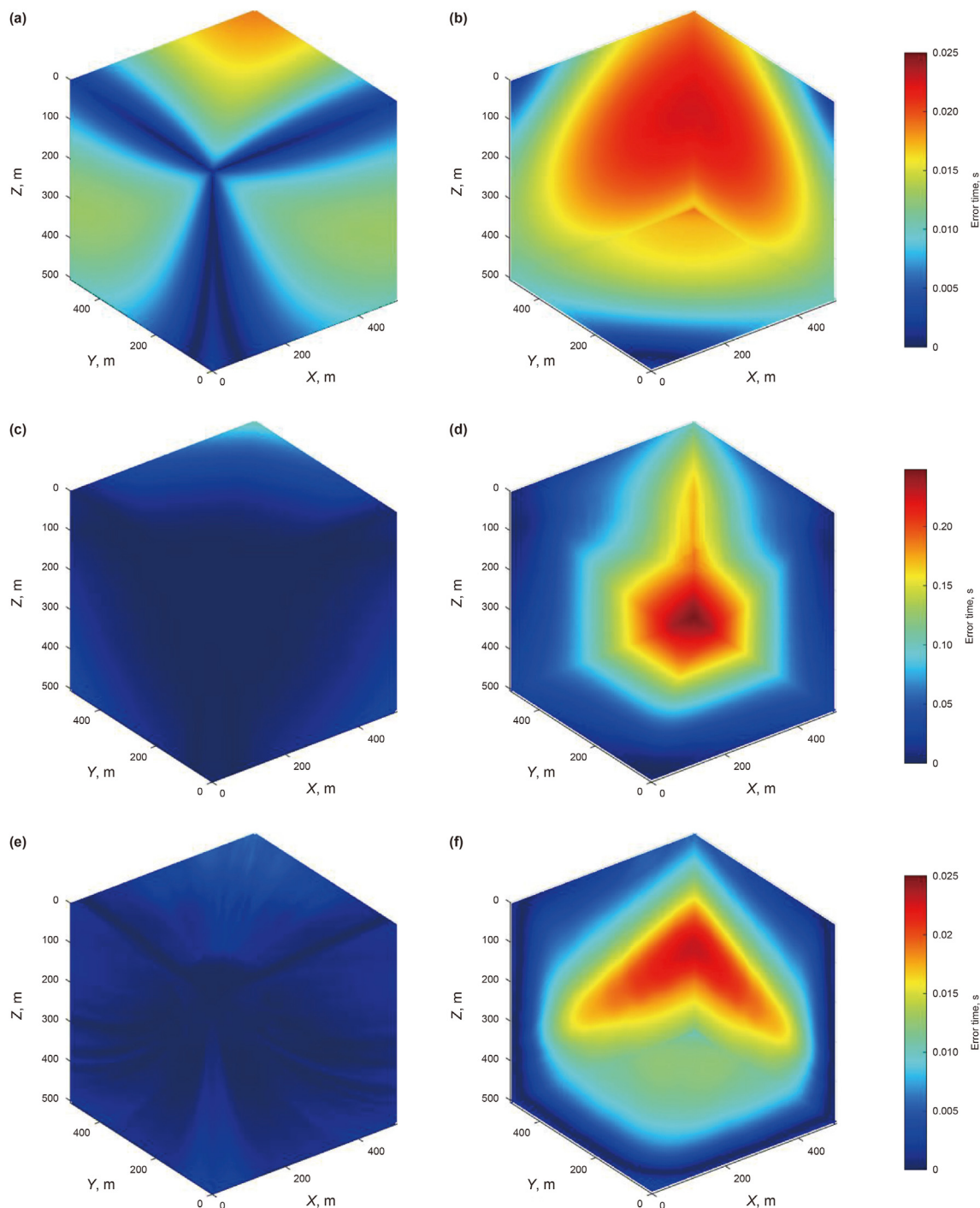


Fig. 8. Absolute traveltimes errors in a 3D model with constant gradient of slowness squared by FS method on faces passing through the grid points (0 m, 0 m, 0 m) (a) and (500 m, 500 m, 500 m) (b), MFD method on faces passing through the grid points (0 m, 0 m, 0 m) (c) and (500 m, 500 m, 500 m) (d) and AFD method on faces passing through the grid points (0 m, 0 m, 0 m) (e) and (500 m, 500 m, 500 m) (f).

Table 2
The maximum absolute traveltimes errors, number of traveltimes errors greater than 0.01 s and computational costs in **example 2**.

Methods	FS	MFD	AFD
Maximum errors, s	2.260E-2	2.483E-1	2.560E-2
Errors >0.01 s, %	85.4	85.5	46.6
CPU time, s	32.473	37.382	16.800

and refracted waves gradually become dominant wave types and the spherical wave operators in AFD method cannot accurately describe the propagations of other wave types, which therefore induces bigger traveltimes errors than FS method for grid point at a long distance from source point as shown in Fig. 8f. Thus, only using local plane wave and refracted wave operators are enough to ensure the accuracy of first-arrival traveltimes calculation at far distance in most situations (Noble et al., 2014). To further improve the accuracy and efficiency, a cubic window with sides of about 100

grid points surrounding source point is adopted for the implementation of AFD method. For grid points locating in the cubic window, all the local operators in AFD method are used to calculate first-arrival traveltimes. For grid points locating outside the cubic window, local operators except for spherical wave operators are used for a more accurate forward modeling. In the following heterogeneous media with sharp slowness variations, the above introduced cubic window also is adopted for AFD method.

4.3. Example 3

In this example, we use the 3D Overthrust model with sharp velocity contrasts to test AFD method for the accurate calculation of first-arrival traveltimes. The size of the 3D model is 10,000 m × 10,000 m × 4675 m with a grid interval of 25 m for each direction. A source locating at the origin coordinate (0 m, 0 m, 0 m) is used to generate the wave fronts as the white lines shown in Fig. 9. It is clearly observed that spherical wave fronts propagating near source point are gradually transformed to plane wave fronts propagating far away from source point in the strongly heterogeneous 3D media. Because the velocity variations along top and bottom faces are smaller than vertical faces, the isochrones on the two horizontal slices are smoother than the isochrones on the other four vertical slices, which indicate an accurate modeling of first-arrival traveltimes. The result is simulated with serial C code running on an intel i7 3.1 GHz and takes a computational cost of 1213 s for the unsmooth 3D Overthrust model, which illustrates that the novel AFD method is efficient for 3D complex realistic model.

5. Discussion

The 3D Overthrust model is a numerical model with sharply varying velocities, which has no analytical solutions of first-arrival traveltimes and thus, the traveltimes error analysis is not adopted in example 3. Based on the identical hardware platform, FS and MFD methods are also tested to calculate first-arrival traveltimes for the 3D Overthrust model with computational costs of 2174 s and 6934 s, respectively. Because AFD method needs the least iteration to converge to the stable solution, both FS and MFD methods take longer time consumptions than AFD method. Meanwhile, plane

wave 8 point operator in AFD method is a more accurate operator than plane wave 2 point operator in FS method, thus, AFD method can characterize plane wave propagation more accurately than FS method. For strongly heterogeneous media, because only spherical wave 2 point operator can not accurately describe the characteristics of all possible seismic wave types, the accuracy of MFD method is lower than that of AFD method with an adaptive selection of different local operators to accurately characterize different seismic wave propagations. Whether from the point of view of computational cost or from the point view of accuracy, AFD method is a better choice for the traveltimes modeling with a more realistic 3D heterogeneous media and will be well applied in scopes such as seismic monitoring, multi-source location and seismic tomographic imaging.

6. Conclusions

In this paper, an accurate adaptive finite-difference (AFD) method is proposed to solve the 3D eikonal equation for seismic first-arrival traveltimes in strongly inhomogeneous media. To improve the numerical accuracy of seismic first-arrival traveltimes in computational domains near source point for fast sweeping (FS) method and far away from source point for multiplicative factor decomposition (MFD) method, our AFD method simultaneously calculates five different local operators to characterize all the possible seismic wave types. Then, the adaptive updating schemes based on the Fermat principle automatically select the most accurate local operator to update both the traveltimes and factors, global fast sweepings along eight directions in 3D domain are adopted to sweep all the possible propagating directions in strongly varying slowness model and Gauss-Seidel iterations guarantee the convergences of numerical solutions. Thus, the novel method can achieve a more accurate modeling of seismic traveltimes than FS and MFD methods for computational domains both near and far away from source point. The three numerical examples further show AFD method is an accurate and stable numerical method, which is better for the calculation of first-arrival traveltimes in 3D media with sharp slowness contrasts.

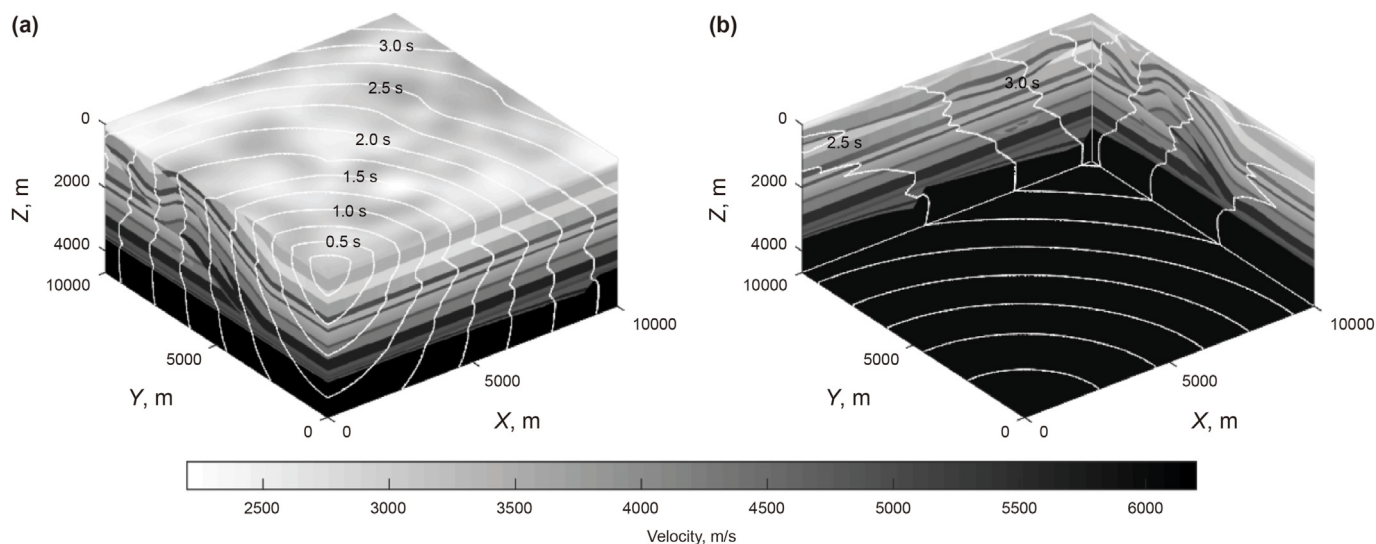


Fig. 9. Overthrust model with a source point located at the origin coordinate (0 m, 0 m, 0 m) generates first-arrival traveltimes with contour plots (white lines) by AFD method on faces passing through the grid points (0 m, 0 m, 0 m) (a) and (10000 m, 10000 m, 4675 m) (b), respectively.

Acknowledgments

The authors thank the funds supported by the China National Nuclear Corporation under Grants Nos. WUQNYC2101 and WUHTLM2101-04, National Natural Science Foundation of China (42074132, 42274154).

References

- Alkhalifah, T., 1998. Acoustic approximations for processing in transversely isotropic media. *Geophysics* 63 (2), 623–631. <https://doi.org/10.1190/1.1444361>.
- Alkhalifah, T., 2003. An acoustic wave equation for orthorhombic anisotropy. *Geophysics* 68 (4), 1169–1172. <https://doi.org/10.1190/1.1598109>.
- Berkar, A.C., Madenci, E., Haghghat, E., et al., 2022. Solving the eikonal equation for compressional and shear waves in anisotropic media using peridynamic differential operator. *Geophys. J. Int.* 229 (3), 1942–1963. <https://doi.org/10.1093/gji/ggac037>.
- Cheng, C., Bodin, T., Allen, R.M., 2016. Three-dimensional pre-stack depth migration of receiver functions with the fast marching method: a Kirchhoff approach. *Geophys. J. Int.* 205 (2), 819–829. <https://doi.org/10.1093/gji/ggw062>.
- Červený, V., Hron, F., 1980. The ray series method and dynamic ray tracing system for three-dimensional inhomogeneous media. *Bull. Seismol. Soc. Am.* 70 (1), 47–77. <https://doi.org/10.1785/BSSA0700010047>.
- Engquist, B., Runborg, O., 2003. Computational high frequency wave propagation. *Acta Numer.* 12, 181–266. <https://doi.org/10.1017/S0962492902000119>.
- Feng, B., Xu, W., Wu, R.S., et al., 2020. Finite-frequency traveltime tomography using the Generalized Rytov approximation. *Geophys. J. Int.* 221 (2), 1412–1426. <https://doi.org/10.1093/gji/ggaa067>.
- Fomel, S., Luo, S., Zhao, H.K., 2009. Fast sweeping method for the factored eikonal equation. *J. Comput. Phys.* 228, 6440–6455. <https://doi.org/10.1016/j.jcp.2009.05.029>.
- Guo, X., Wang, J., Yang, S., et al., 2022. Optimal staggered-grid finite-difference method for wave modeling based on artificial neural networks. *Comput. Math. Appl.* 108, 141–158. <https://doi.org/10.1016/j.camwa.2022.01.012>.
- Hao, Q., Alkhalifah, T., 2017a. An acoustic eikonal equation for attenuating transversely isotropic media with a vertical symmetry axis. *Geophysics* 82 (1), C9–C20. <https://doi.org/10.1190/geo2016-0160.1>.
- Hao, Q., Alkhalifah, T., 2017b. An acoustic eikonal equation for attenuating orthorhombic media. *Geophysics* 82 (4), WA67–WA81. <https://doi.org/10.1190/geo2016-0632.1>.
- Kao, C.Y., Osher, S., Tsai, Y.H., 2005. Fast sweeping methods for static Hamilton-Jacobi equations. *SIAM J. Numer. Anal.* 42 (6), 2612–2632. <https://doi.org/10.1137/S003614290241960>.
- Li, L., Becker, D., Chen, H., et al., 2018. A systematic analysis of correlation-based seismic location methods. *Geophys. J. Int.* 212 (1), 659–678. <https://doi.org/10.1093/gji/ggx436>.
- Li, Z., Huang, Q., 2014. Application of the complex frequency shifted perfectly matched layer absorbing boundary conditions in transient electromagnetic method modeling. *Chin. J. Geophys.* 57 (4), 1292–1299. <https://doi.org/10.6038/cjg20140426> (in Chinese).
- Lu, Y., Zhang, W., 2022. Calculating the traveltimes of qSV and qSH waves using fast sweeping method for 2D VTI media by solving quadratic equation. *Chin. J. Geophys.* 65 (1), 244–255. <https://doi.org/10.6038/cjg202200446> (in Chinese).
- Meléndez, A., Korenaga, J., Sallarès, V., Miniussi, A., et al., 2015. TOMO3D: 3-D joint refraction and reflection traveltime tomography parallel code for active-source seismic data—synthetic test. *Geophys. J. Int.* 203 (1), 158–174. <https://doi.org/10.1093/gji/ggv292>.
- Noble, M., Gesret, A., Belayouni, N., 2014. Accurate 3-D finite difference computation of traveltimes in strongly heterogeneous media. *Geophys. J. Int.* 199 (3), 1572–1585. <https://doi.org/10.1093/gji/ggu358>.
- Podvin, P., Lecomte, I., 1991. Finite difference computation of traveltimes in very contrasted velocity models: a massively parallel approach and its associated tools. *Geophys. J. Int.* 105 (1), 271–284. <https://doi.org/10.1111/j.1365-246X.1991.tb03461.x>.
- Qiao, B., Pan, Z., Huang, W., et al., 2021. An adaptive finite-difference method for accurate simulation of first arrival traveltimes in heterogeneous media. *Appl. Math. Comput.* 394, 125792. <https://doi.org/10.1016/j.amc.2020.125792>.
- Sethian, J.A., 1996. A fast marching level set method for monotonically advancing fronts. *Proc. Natl. Acad. Sci. U.S.A.* 93, 1591–1595. <https://doi.org/10.1073/pnas.93.4.159>.
- Stovas, A., Alkhalifah, T., 2012. A new traveltime approximation for TI media. *Geophysics* 77 (4), C37–C42. <https://doi.org/10.1190/geo2011-0158.1>.
- Stovas, A., 2015. Azimuthally dependent kinematic properties of orthorhombic media. *Geophysics* 80 (6), C107–C122. <https://doi.org/10.1190/geo2015-0288.1>.
- Tan, Y., Hu, J., Zhang, H., et al., 2020. Hydraulic fracturing induced seismicity in the southern sichuan basin due to fluid diffusion inferred from seismic and injection data analysis. *Geophys. Res. Lett.* 47 (4), e2019GL084885. <https://doi.org/10.1029/2019GL084885>.
- Thorbecke, J.W., Draganov, D., 2011. Finite-difference modeling experiments for seismic interferometry. *Geophysics* 76 (6), H1–H18. <https://doi.org/10.1190/geo2010-0039.1>.
- Vidale, J., 1988. Finite-difference calculation of travel times. *Bull. Seismol. Soc. Am.* 78 (6), 2062–2076. <https://doi.org/10.1785/BSSA0780062062>.
- Vidale, J., 1990. Finite-difference calculation of travel times in three dimensions. *Geophysics* 55 (5), 521–526. <https://doi.org/10.1190/1.1442863>.
- Waheed, U.B., Haghghat, E., Alkhalifah, T., et al., 2021. PINNeik: eikonal solution using physics-informed neural networks. *Comput. Geosci.* 155, 104833. <https://doi.org/10.1016/j.cageo.2021.104833>.
- Yang, H., Zhang, J., Ren, K., et al., 2021. First-arrival traveltime inversion of seismic diving waves observed on undulant surface. *Geophys. J. Int.* 225 (2), 1020–1031. <https://doi.org/10.1093/gji/ggab025>.
- Zhao, H.K., 2005. A fast sweeping method for eikonal equations. *Math. Comput.* 74 (250), 603–627. <https://doi.org/10.1090/S0025-5718-04-01678-3>.
- Zhu, X., Gao, R., Li, Q., et al., 2014. Static corrections methods in the processing of deep reflection seismic data. *J. Earth Sci.* 25 (2), 299–308. <https://doi.org/10.1007/s12583-014-0422-x>.